The Cryosphere Discuss., 7, 2061–2088, 2013
www.the-cryosphere-discuss.net/7/2061/2013/
doi:10.5194/tcd-7-2061-2013

The Cryosphere Discussions
Open Access

Characterization of L-band synthetic aperture radar (SAR) backscatter from floating and grounded lake ice in arctic Alaska

M. Engram[1], K. W. Anthony[1], F. J. Meyer[2], and G. Grosse[3]

[1]Water and Environmental Research Center, Institute of Northern Engineering, University of Alaska Fairbanks, 306 Tanana Loop, Fairbanks, AK 99775-7000, USA
[2]Earth & Planetary Remote Sensing, Geophysical Institute, University of Alaska Fairbanks, 903 Koyukuk Dr., Fairbanks, AK 99775-7000, USA
[3]Permafrost Laboratory, Geophysical Institute, University of Alaska Fairbanks, 903 Koyukuk Dr., Fairbanks, AK 99775-7000, USA

Received: 6 April 2013 – Accepted: 2 May 2013 – Published: 22 May 2013

Correspondence to: M. Engram (melanie.engram@alaska.edu)

Published by Copernicus Publications on behalf of the European Geosciences Union.

Abstract

Synthetic aperture radar (SAR) backscatter from floating lake ice is high, in contrast to low backscatter values from lake ice that is frozen completely to the lake bed (grounded ice). Knowledge of floating vs. grounded lake ice is useful for determining winter water supply, fish habitat, heat transfer to permafrost, and to observe changes in perennial lake ice status that could correlate with variations in local climate. Here, we compare calibrated L-band (23.6 cm wavelength) single- and L-band quadrature-polarized SAR return to the backscatter intensity of C-band (5.6 cm wavelength) SAR from floating and grounded lake ice over two regions in Alaska. Our primary goal was to determine if C or L-band is more useful to distinguish floating from grounded lake ice. C-band SAR showed far greater contrast between floating and grounded lake ice, making it the preferred wavelength for identifying lake ice regimes. L-band SAR backscatter was much lower from floating ice than C-band and it was different for our two study regions. Furthermore, since L-band is sensitive to ebullition bubbles trapped by lake ice (bubbles increase backscatter), this study helps to elucidate potential confounding factors of bubbles in efforts to detect floating vs. grounded ice using L-band SAR.

1 Introduction and background

Thermokarst (thaw) lakes are abundant in arctic and sub-arctic permafrost lowlands, comprising more than 40 % of the land area in some regions (Grosse et al., 2013). Formed by thermal degradation of permafrost and melting of ground ice, thermokarst lakes range in depth from 1–2 m to more than 10 m, largely depending on the ice content of the permafrost in the region and on lake age.

Seasonal ice-cover typically starts forming on lake surfaces in late October or early November in arctic Alaska and grows to a maximum thickness of over one meter to two meters by late March/early April (Mellor, 1982; Jeffries et al., 1994). Some lakes are shallower than 1–2 m and no liquid water remains under the ice at maximum seasonal

TCD
7, 2061–2088, 2013

ice thickness, resulting in grounded ice. In lakes that are deeper than the maximum ice thickness, liquid water remains under the thick ice cover all winter (floating ice). Other lakes have a shallow littoral region and freeze to the lake bed close to the shore, while ice floats on liquid-phase water in deeper lake centers.

Using SAR remote sensing to determine floating or grounded lake ice is useful in the Arctic, where in situ field measurements are costly and difficult. SAR backscatter from newly formed and thickening lake ice in thermokarst lakes has been well documented for C-band frequency (Jeffries et al., 1994; Duguay et al., 2002): backscatter intensity after initial ice formation is very low (< −15 dB), and cracks in thin ice can be detected (Hall et al., 1994); however, SAR intensity quickly increases as ice thickens throughout the winter to reach a ceiling of −6 to −7 dB for floating ice. If lake ice grows thick enough to completely ground to the lake bed, the SAR backscatter intensity is low (−14 to −18 dB).

Distinguishing whether or not lakes freeze completely to the lake bed is useful for a multitude of reasons: to identify fish over-wintering habitat, to identify winter water availability for domestic water supply to rural villages or winter ice roads, to determine lakes that show a sudden drop in water level due to partial drainage. Ice monitoring from year to year can be used as an indicator of climate change (Hall et al., 1994; Morris et al., 1995) and as an indicator of permafrost health, since an increase in floating lake ice area alters heat flux on the thermokarst-lake landscape regimes (Jeffries et al., 2002; Arp et al., 2011, 2012). Finally, the magnitude of backscatter intensity decrease that suddenly occurs when lakes freeze to the lake bed is important to know in order to eliminate lakes that exhibit a backscatter drop of this magnitude from lake ice analyses targeting methane ebullition (Engram et al., 2012).

Determining which combination of SAR parameters of wavelength, incidence angle and polarization works best to distinguish between floating and grounded lake ice is an important precondition for targeted or operational lake ice studies. SAR, as an active instrument, does not continually acquire data and SAR satellites have a finite lifetime. These two factors result in temporal imaging gaps by particular sensors in data

TCD
7, 2061–2088, 2013

archives. The resulting history of available SAR data over any particular area is therefore often a mixture of X, C and L-bands with different incidence angles and different polarizations.

The high contrast of microwave backscatter from floating lake ice versus grounded lake ice was first discovered in the late 1970's with X-band Side Looking real-aperture Airborne Radar (SLAR) (Sellmann et al., 1975; Elachi et al., 1976; Weeks, 1977). Coastal land areas with lakes were imaged during sea-ice imaging missions. At least two SLAR missions used L-band as well as X-band microwave backscatter and qualitative examination of SLAR images found that both wavelengths had high return from floating ice and low return from grounded ice (Elachi et al., 1976; Sellmann et al., 1977). Elachi et al. (1976) noticed a larger contrast between floating and grounded ice from L-band than X-band in uncalibrated SLAR.

The same phenomenon of high-backscatter return from floating ice and low return from grounded ice was observed in the early 1990's with the advent of calibrated spaceborne SAR, using the C-band VV microwave signal of ERS-1 and ERS-2 (Jeffries et al., 1994; Morris et al., 1995; French et al., 2004). Others have observed this difference using Radarsat-1 C-band HH data (Duguay et al., 2002; Hirose et al., 2008; Arp et al., 2011). Duguay et al. (2002) additionally examined the effect of a varying incidence angle on lake ice and found that a steeper incidence angle (20°–35°) provided higher backscatter values from floating ice than a shallow incidence angle (35°–49°) for calibrated C-band HH SAR, and that this difference was more pronounced from ice with fewer tubular bubbles. Evaluating high or low C-band SAR backscatter from lake ice has become an established method for determining whether a lake retains floating ice all winter or if lake ice is frozen completely to the lake bed in arctic and sub-arctic lakes (Jeffries et al., 1996; French et al., 2004; White et al., 2008; Arp et al., 2012).

One of the main drivers of radar backscatter intensity is the dielectric constant of the target. Liquid water has a very large real dielectric constant (ε') compared to ice, so the water–ice interface with its high dielectric contrast has been an obvious explanation for part of the radar return from floating ice. For L-band, $\varepsilon \approx 88$ for cold water (Skolunov,

TCD
7, 2061–2088, 2013

1997) and for C-band, $\varepsilon' \approx 69$, while ice has a dielectric constant of 3.2 for both C- and L-band wavelengths (Leconte et al., 2009). Because of this large difference in the magnitude of ε' for ice and water, there is a strong reflectance of both C and L-band microwave from the ice-water interface.

A smooth liquid water surface will reflect microwaves away from the receiving antenna on the satellite due to specular reflection, as demonstrated by calm open water or by newly frozen lakes that appear black in a SAR image. An additional reflector must be present for energy to be turned once again and reflected back to the satellite. Weeks (1978, 1981) and others (Jeffries et al., 1994; Mellor, 1982; Morris et al., 1985; Duguay et al., 2002) have posited that the small tubular bubbles formed in lake ice by the rejection of dissolved gasses during the freezing process (Gow and Langson, 1977; Boereboom et al., 2012) play a role in turning radar back to the satellite. Similarly, Engram et al. (2012) showed a positive correlation between L-band backscatter and the abundance of ebullition bubbles in ice-covered lakes. The same study demonstrated that this positive correlation between single-pol L-band SAR and field measurements of ebullition bubbles in frozen lakes did not exist for C-band VV SAR. Further, they used a polarimetric decomposition to posit that free-phase gas bubbles trapped under ice create a rough surface that interacts with Band 3 of the Pauli decomposition (Cloude and Pottier, 1996), resulting in a strong reflectance back to the satellite.

It should be noted that some dark areas on lake ice in uncalibrated SAR images have been documented for floating ice on deep lakes (130 m) in Montana, USA (Hall et al., 1994). Hall et al. (1994) attributed these dark areas to thinner ice in zones of the lake that had more snow cover and to the different stratigraphy of small tubular bubbles in lake ice than that of northern Alaskan thermokarst lakes. Lakes in more temperate climates have later freeze-up, thinner ice, slower ice growth, possibly more white ice, different patterns of tubular bubbles (Hall et al., 1994) and possibly thawing and refreezing events during the winter. Dark areas of low backscatter return from these lakes would not indicate grounded ice, but could instead indicate thin, newly-formed ice or ice without small tubular bubbles near the ice/water interface (Hall et al., 1994).

TCD
7, 2061–2088, 2013

Here we examine the value of single-polarized (single-pol) L-band HH backscatter from floating and grounded lake ice compared to C-band VV SAR values to determine its utility in distinguishing between grounded and floating ice. We use a polarimetric decomposition of quadrature-polarized (quad-pol) SAR to ascertain which scattering mechanism (roughness, double-bounce or volumetric scattering) or combination of mechanisms is displayed by floating lake ice for Advanced Land Observing Satellite (ALOS) PALSAR L-band SAR. We statistically test the means of backscatter intensity for equality from ice on lakes within a region and between regions. Finally, we characterize the difference in L-band backscatter intensity between floating ice and grounded ice for single-pol (HH) and the $T11$, $T22$ and $T33$ polarimetric elements from the coherency matrix of a decomposed quad-pol SAR signal (Lee and Pottier, 2009).

2 Methods

2.1 Study areas

We extracted backscatter values from SAR images of floating and grounded ice from lakes in two regions in Alaska, USA: the northern Seward Peninsula (NSP) (≈ 66.5° N, 164.4° W, five lakes) and the Arctic Coastal Plain (ACP), south of Barrow, Alaska (≈ 71.2° N, 156.6° W, six lakes) (Fig. 1). Both are coastal regions (Fig. 1), but they differ in permafrost and climatic characteristics and therefore contain two distinct types of thermokarst lakes. Permafrost on the northern Seward Peninsula is generally less thick (ca. 100 m) than on the Arctic Coastal Plain (up to 600 m) (Jorgenson et al., 2008). The near surface layer of ice-rich permafrost is thicker (> 20 m) on the northern Seward Peninsula (West and Plug, 2008) than on the Arctic Coastal Plain (< 5 m) (Jorgenson and Shur, 2007), resulting in deeper lakes when ground ice melts. The deep soil organic carbon stocks in the ice-rich Yedoma deposits on the northern Seward Peninsula potentially are also higher than soil carbon stocks in the deeper marine, fluvial, and eolian deposits on the Arctic Coastal Plain (Walter Anthony, unpublished data).

TCD
7, 2061–2088, 2013

As a result, thermokarst lakes on the northern Seward Peninsula have a higher rate of methane production, resulting in a larger abundance of ebullition bubbles trapped in and under lake ice (Walter Anthony and Anthony, 2013). In contrast, lakes south of Barrow on the Arctic Coastal Plain have significantly fewer ebullition bubbles included in their ice cover (Walter Anthony et al., 2012). Including lakes with both high and low numbers of ebullition bubbles was important to this study since ebullition may be a confounding factor in isolating floating and grounded ice values in L-band imagery.

Field data on lake ice thickness was collected for four NSP thermokarst lakes in April 2009 that varied both in bathymetry (deep vs. shallow) and in levels of ebullition bubbles observed previously by Engram et al. (2012) in field work. In addition, we included in this study the larger Whitefish Maar, a 6 m deep lake on the NSP of volcanic origin that does not freeze to bottom in the center (Hopkins et al., 1988). We identified areas of grounded and floating ice on the NSP study lakes using both field measurements and recent ERS-2 image interpretation. To identify areas of lakes with grounded vs. floating lake ice on the ACP, we used the ERS-2 signal and data from previous work that established C-band VV signal for floating and grounded ice (Mellor, 1983; Jeffries, 1996). Five of the six Arctic Coastal Plain study lakes were featured in early radar research (Sellmann et al., 1975; Mellor, 1982; Jeffries et al., 1994). We chose one other lake to increase the sample sizes of lakes with either floating or grounded ice based on recent ERS-2 SAR imagery.

2.2 SAR imagery

We sampled pixels from L-band Japanese Earth Resources Satellite-1 (JERS-1) scenes from 1993–1998 and from both single- and quad-pol L-band PALSAR scenes acquired during 2008–2011 in spring (late March to early April; Table 1). We selected this spring time frame since it represents the period of maximum lake ice thickness while preceding the onset of melting. ERS-1 and ERS-2 C-band SAR scenes were selected based on acquisition dates closest to L-band SAR acquisitions for verification of grounded lake ice conditions and for comparison of L-band with C-band SAR. The

TCD
7, 2061–2088, 2013

C-band scenes were generally acquired on either the same day or just a few days apart from L-band acquisitions. Exceptions to this rule are two cases where a week or more lapsed between acquisitions from the different sensors (Table 1). We used PolSARpro software (v. 4.2.0) to decompose quad-pol L-band images into the 3 × 3 complex coherency matrix [$\mathbf{T}_3$], and compared the $T11$, $T22$, and $T33$ elements of the coherency matrix (Lee and Pottier, 2009) to SAR single-pol intensity values (Gao, 2010). The $T11$, $T22$ and $T33$ polarimetric elements are equivalent to the spatially averaged versions of Band 3, Band 1, and Band 2 of a Pauli decomposition (Claude and Pottier, 1996), although generally the Pauli bands are expressed as amplitude, which is the square root of the intensity images used in this study. Polarimetric decompositions, such as the Pauli decomposition, provide information about the scattering mechanisms of point and distributed targets by examining the polarization state of transmitted and received energy with the complex scattering matrix [**S**] (Cloude, 2010; van Zyl and Kim, 2010).

2.3 GIS sample methods

Shallow lakes freeze to the bottom completely and appear dark in a SAR image. Others lakes are deep enough that no part of the lake freezes to the bottom, except a narrow border near the shore that is less than one pixel and therefore not visible in SAR imagery. Still other lakes have wide shallow littoral zones that freeze completely to the lake bed while ice in deeper areas of the lake remains floating, producing a dark lake margin in a SAR image with a bright lake center. Clearly, using all of the pixels from a lake would not be useful if lake ice was partially grounded and partially floating. To exclude mixed pixels with grounded and floating ice from the analysis, we developed a supervised selection method to identify a large number of pixels that were either entirely floating or grounded ice from the same locations within lakes on co-registered SAR images. Using a manual interpretation of ERS-2 imagery and field ice-thickness measurements from April 2009, we classified areas of frozen lakes for both study sites as (1) grounded ice, (2) floating ice, or (3) an ambiguous area. We used ERS-2 imagery that was as co-temporal as possible to L-band SAR from JERS-1 and PALSAR.

TCD
7, 2061–2088, 2013

We created straight lines in GIS within a particular ice type (floating or grounded) on an ERS-1 or -2 image, then sampled pixels near uniformly spaced points along these sample lines using bilinear interpolation (Fig. 2). For consistency, the number of pixels we sampled was related to lake area: we created sample lines so that the ratio of sample line length to lake area was 25–35 m per square kilometer of lake surface. The resulting spacing between sample lines and between uniformly spaced points ensured that 18 m pixels would not be sampled twice. This method of supervised sampling allowed us to preclude ambiguous portions of lakes that could not be classified, using C-band SAR images, as either floating or grounded ice. We refined the geolocation of the SAR images in GIS using lateral translation to ground control points, then selected pixels from the same geographic locations on each SAR image in the stack with uniform points along sample lines with the ArcGIS™ Sample Tool.

We used the Shapiro–Wilk Test to determine normality on all data distributions. We compared both grounded and floating ice backscatter between our two study regions using a statistical *t* test for each SAR imaging parameter (wavelength/polarization combinations). All statistics were determined by SPSS (v. 19) software. To determine which SAR wavelength/polarization combination was most useful to distinguish floating and grounded lake ice, we compared the difference between floating and grounded lake ice backscatter values to find the SAR imaging parameters that exhibited the most contrast.

3 Results

SAR backscatter values were consistent between years for late March/April scenes for all imaging parameters: box-plots of distributions showed no far-outliers, and only one case of a near-outlier (Fig. 3). Backscatter values of sampled pixels for floating and grounded ice averaged from individual lakes in each SAR scene were normally distributed (Shapiro–Wilk, $\alpha = 0.05$).

TCD
7, 2061–2088, 2013

From grounded ice SAR backscatter intensity was very low (< −14 dB) for all imaging parameters for both NSP and ACP regions (Fig. 4). The average SAR radar cross section of grounded ice for single-pol L-band was −19 dB for both ACP and NSP (Table 2). This was significantly lower than the average C-band grounded ice intensity of −15 dB for ACP and −14 dB for NSP ($p < 0.01$). Backscatter intensity from quad-pol L-band SAR for grounded lake ice, when decomposed into polarimetric elements, was highest (−16 dB) for $T11$ (roughness) for both regions, intermediate for $T22$ (double-bounce) with −20 dB (ACP) and −23 dB (NSP), and lowest for $T33$ (volume scattering) with −25 dB (ACP) and −27 dB (NSP) (Table 2). A statistical t test showed that the average radar brightness of grounded ice on the ACP was not different for C-band vs. the L-band $T11$ (roughness) component. On the NSP however, means of these two parameters for grounded ice were statistically different ($p < 0.01$). Backscatter intensity from grounded ice on the ACP was significantly different than from the NSP for C-band ($p < 0.01$) and L-band $T22$ (double bounce) ($p < 0.04$). A t test failed to reveal a statistically significant difference between the two regions for grounded ice in L-band HH, L-band $T11$ (roughness), and $T33$ (volumetric); therefore we assumed equal means (Table 2).

For floating ice, C-band VV backscatter values were statistically identical for both regions (−6 dB) and substantially higher than L-band values for single-pol and all polarimetric scattering components (Table 2). L-band single-pol (HH) backscatter values from floating lake ice showed statistically significant regional variability and were higher on the NSP (−13 dB) than the ACP (−16 dB). The roughness polarimetric element ($T11$) of quad-pol L-band SAR was the highest returned signal for floating ice for L-band SAR with a mean backscatter of −9 dB on the NSP and −12 dB on the ACP. In comparison, the values of the polarimetric elements representing double-bounce ($T22$) and volumetric scattering ($T33$) were low for floating ice on both regions: −17 dB to −20 dB for $T22$, and −21 dB to −24 dB for $T33$ (Table 2 and Fig. 4). Polarimetric element $T11$ (roughness) was significantly higher for floating ice from lakes in the NSP

TCD
7, 2061–2088, 2013

than from lakes in the ACP ($p < 0.01$), but $T22$ (double-bounce) and $T33$ (volumetric) were lower from floating ice in the NSP than ACP (Table 2 and Fig. 4).

The contrast (arithmetic difference) between floating and grounded ice SAR backscatter was determined by subtracting the grounded-ice sigma-naught backscatter intensity value from that of floating ice, using linear powerscale units. This floating/grounded ice difference was largest in C-band with a mean intensity difference between these two ice types of 0.20 (powerscale) on the NSP and 0.23 (powerscale) on the ACP (Fig. 5). While the logarithmic scale of decibels prohibits directly subtracting dB values, this C-band contrast was the result of the difference between the floating ice mean of −6 dB to the grounded ice mean of −14 dB and −15 dB for lakes on the NSP and ACP respectively. L-band HH contrast between floating and grounded ice in both regions was much lower than C-band contrast, with an L-band mean intensity difference between floating and grounded ice of 0.035 on the NSP and 0.009 on the ACP. These single-pol L-band powerscale values, when converted to decibel log-scale, were the difference between the mean floating and grounded ice intensities of −13 dB and −19 dB on the NSP, −16 dB and −19 dB on the ACP (Table 2).

For all decomposed elements of quad-pol L-band data, backscatter from grounded ice was always lower than from floating ice, but the difference in powerscale units between floating and grounded ice was very small (< 0.01) for $T22$ (double-bounce) and even smaller (< 0.005) for $T33$ (volumetric). The difference between the means of floating and grounded ice for $T11$ (roughness) was largest of the three polarimetric elements, 0.05 for the ACP, and 0.10, twice as large as for ACP, for the NSP (Fig. 5).

During the time frame of this study, 1993–2011, we noticed that many lakes flipped from springtime grounded-ice to floating-ice status and a few changed from floating ice to grounded ice status. Some lakes in the ACP region froze to the bottom in the 1990's but no longer freeze to the bottom in the late 2000's (based on recent C-band SAR data). For example, one of the study lakes, West Twin Lake, was frozen to the lake bed in the 1992 and 1998 spring images, but in 2008 spring images, C-band radar backscatter of about −6 dB signified floating ice. Another study lake on the ACP,

TCD
7, 2061–2088, 2013

Kimouksik Lake, was a floating-ice lake in 1993, but low SAR backscatter evinced Kimouksik ice was freezing to the bottom in 2008.

4 Discussion

4.1 Grounded ice

We found higher backscatter from grounded ice in C-band (−14 to −15 dB) than in single-pol L-band (−19 dB). The fact that SAR backscatter was very low from grounded ice for L-band HH is most likely explained by the low dielectric contrast at the ice-soil interface on the lake bottom. This has been well documented in studies of uncalibrated airborne L-band radar return (Elachi et al., 1976; Weeks, 1978). In the case of grounded lake ice, microwaves pass through snow and lake ice, but with no liquid-phase water to provide a high dielectric contrast, most of the radar is absorbed by the lake bed instead of reflected back to the satellite. The reason for a higher response from C-band vs. L-band from grounded ice could be that C-band was reflecting from small inclusions in the ice, such as tubular bubbles, that are too small to create a significant scattering contribution in L-band. Another reason could be that C-band is picking up small scale roughness patterns of the lake bottom that are less relevant for the longer L-band wavelength. Roughness is a quality that is wavelength-dependent: the smaller the SAR wavelength, the smaller vertical height variations can cause backscatter return from roughness (Ulaby et al., 1986). Also, L-band could return less backscatter from grounded ice because of more effective penetration into the frozen ground: penetration into a medium is also wavelength dependent with the longer wavelength of L-band penetrating deeper than does C-band with a shorter wavelength.

For L-band, the signal from grounded ice was a combination of mostly roughness (−16 dB) with some contribution from double-bounce (< −20 dB), while volumetric scattering was negligible (≤ −25 dB), indicating that volumetric scattering from ice itself, in the absence of liquid water below the ice, is close to the noise level of the data (Fig. 4c).

TCD
7, 2061–2088, 2013

This relatively higher L-band $T11$ roughness backscatter from grounded lake ice could be explained by the presence of rocks or other forms of roughness on the frozen lake-bed. The small contribution from $T22$ (double-bounce) could be explained by L-band reflecting from the lake bed, then reflecting again from bubbles in the lake ice.

The roughness component for L-band, $T11$ from grounded ice was −16 dB for both regions, while C-band VV backscatter for grounded ice was statistically significantly higher from NSP lakes than for ACP (Table 2). A polarimetric analysis of C-band quad-pol data, not available in this study, would be needed to determine which scattering mechanisms are in play for grounded ice with C-band.

4.2 Floating ice

Floating ice values from polarimetric roughness parameter $T11$ indicate that roughness appears to be the dominant scattering mechanism in L-band for floating lake ice in these two permafrost regions (Fig. 4c). The contributions from double-bounce and volumetric scattering are both significantly smaller. Polarimetric element $T11$, indicating roughness as scattering mechanism, is significantly higher in lakes on the NSP compared to the ACP region. The opposite is true of $T22$ (double-bounce) and $T33$ (volumetric), which are slightly but significantly higher on the ACP. One reason for higher backscatter in the roughness component from NSP lake ice could be the higher rate of ebullition bubbling from lakes in the NSP area (Engram et al., 2012; Walter Anthony and Anthony, 2013).

Floating ice L-band single-pol HH was also significantly higher from lakes on the NSP (−9 dB) than from floating lake ice on the ACP (−12 dB). Differences in ebullition bubbling activity in lakes between these two regions most likely explain this difference. Lakes on the NSP have a higher concentration of ebullition bubbles than ACP area lakes (Engram et al., 2012; Walter Anthony et al., 2012; Walter Anthony and Anthony 2013). The findings that L-band single-pol and $T11$ roughness component from floating ice are higher in the NSP then the ACP corroborate the relationship between L-band backscatter and methane flux documented by Engram et al. (2012).

TCD
7, 2061–2088, 2013

While C-band VV shows a much higher intensity from floating ice than L-band, we cannot determine the scattering mechanism that drives this high return without a polarimetric analysis of quad-pol C-band SAR. We recommend such polarimetric analysis for the C-band wavelength to see what is driving the high backscatter signal from floating ice at this wavelength. High backscatter intensity from single-pol C-band has been closely associated with small tubular bubbles formed in lake ice as dissolved gasses are rejected during the freezing process as well as with the high dielectric contrast at the ice/water interface (Weeks et al., 1978). These tubular bubbles, combined with the ice/water interface could conceivably cause double-bounce (Mellor, 1982; Weeks et al., 1981) or roughness scattering (Weeks, et al., 1978).

C-band SAR is more sensitive to smaller height variations in a rough surface than L-band SAR, due to its shorter wavelength. High backscatter values (−4 to −7 dB) from floating lake ice from C-band VV 23° SAR, as reported in this and other studies (Morris et al., 1995; Jeffries et al., 1994) and C-band HH SAR, as reported by Duguay et al. (2002) could be caused in whole or in part by a rough target with "roughness" dimensions too small to be picked up by L-band SAR. If small tubular bubbles cause roughness at the water/ice interface, a scenario that Weeks et al. (1978) suggest as a possibility, then roughness at the water surface from vertically oriented tubular bubbles could be too small to detect with L-band, yet could cause the high backscatter from floating ice for C-band SAR.

4.3 Comparison of C-band and L-band for detecting grounded ice

The difference in magnitude of C-band backscatter between floating and grounded ice was five to thirty-six times higher than the floating-to-grounded ice difference in single-pol L-band (Fig. 5), mostly due to the very high backscatter intensity (−6 dB) from floating ice in C-band. This greater contrast between floating and grounded ice makes C-band VV a more useful tool to distinguish grounded from floating lake ice than L-band SAR. Even the L-band parameter that showed the highest contrast between

TCD
7, 2061–2088, 2013

floating and grounded ice, the $T11$ roughness component, showed less than half of the contrast than C-band VV showed between floating and grounded ice.

Another advantage of C-band VV in distinguishing grounded vs. floating ice is that it is less sensitive to ebullition bubbles trapped by lake ice. In contrast, the L-band signal is sensitive to ebullition bubbles trapped by lake ice, which appear to confound the freeze-to-bottom signal response in L-band. In a study of lakes containing different levels of ebullition activity, Engram et al. (2012) observed a positive correlation between backscatter and abundance of ebullition bubbles associated with lake ice for L-band single-pol and the roughness component in the Pauli decomposition (analogous to $\sqrt{T11}$). Similarly, we found higher backscatter in these L-band parameters over high ebullition areas within individual lakes. Figure 6 shows examples of the L-band responses to ebullition and grounded ice in one NSP lake. This higher L-band backscatter response from lake ice with trapped ebullition bubbles confounds a clear distinction between floating and grounded lake ice. Conversely, grounded lake ice can be a confounding factor for detecting and quantifying ebullition activity in lakes using L-band SAR. The freeze-to-the-bottom decrease in backscatter can be avoided in ebullition studies by omitting lakes that show a spring decrease in backscatter, although this precludes a lot of spring ice from analysis. C-band is not sensitive to the presence of ebullition bubbles trapped by lake ice (Engram et al., 2012).

While performing this analysis, we noticed many lakes on the ACP, West Twin Lake for example, that froze to the bottom in the 1990's did not freeze to the bottom in the 2000's images. This could be explained by warmer winters, or winters with more insulating snowfall in the more recent past (Walsh et al., 1998; Duguay et al., 2003; Brown and Duguay, 2010). Our observations corroborate the same shift from grounded to floating lake ice regimes on the Alaska ACP that has been well documented by Arp et al. (2012), even though our study area on the Alaska ACP is to the northwest of the Arp et al. (2012) study lakes. Both snow fall and warmer mean temperature anomalies have increased at Barrow since 1990, resulting in thinner lake ice on the ACP (Arp et al., 2012). Using SAR backscatter to identify whether thermokarst lakes have floating

TCD
7, 2061–2088, 2013

ice or freeze to the bottom will also aid identification of lakes with potential taliks (thaw bulbs) versus frozen bottom sediments, respectively, and thus may provide a useful classification parameter correlating with methane emission of lakes in a region. For example, Arp et al. (2012) suggest that a transition from grounded ice lakes to floating ice lakes observed for the Alaska Coastal Plain may result in enhanced thermokarst activity and talik formation.

Kimouksik Lake, the large ACP lake that exhibited floating ice in the 1990's, yet can be seen as freezing to bottom in 2008, is an example of an opposite trend in ice grounding patterns over decadal time scales. This switch from floating ice to grounded ice was a result of a change in water level due to the draining of an adjacent lake between 1992 and 2002. The hydrological changes of this lake are well documented in Jones (2006). This lake demonstrates the ability of a simple and fast SAR classification of floating and grounded ice to quickly pin-point partial lake drainage events that result in a reversal of floating to grounded ice.

5 Conclusions

SAR is useful for monitoring the status of arctic and sub-arctic lakes seasonally freezing to the bottom, as seen by the example of Kimouksik Lake in the ACP. Future work should include assessment and inventory of lakes that change status from grounded to floating as an indicator of climate change or from floating to grounded ice, as an indicator of water-level lowering.

C-band VV is more suitable than L-band (either single-pol or decomposed quad-pol SAR) for distinguishing between lakes that freeze to the bottom and lakes with floating ice for two reasons, (1) it shows greater contrast between floating and bed-fast ice and (2) because L-band is more sensitive to ebullition bubbles.

The scattering mechanism for floating lake ice in L-band is primarily roughness. Future work should include a similar polarimetric analysis of C-band SAR to determine scattering mechanism(s) for floating lake ice for this shorter wavelength.

TCD
7, 2061–2088, 2013

Acknowledgements. We acknowledge the Alaska Satellite Facility (ASF), both the NASA's Distributed Data Archive Center and JAXA's (Japan Aerospace exploration Agency's) Americas ALOS Data Node for access to SAR data. Access to field sites on the Bering Land Bridge National Preserve was granted by the National Parks Service (permit # BELA-2008-SCI-0002). Funding was provided by NASA Carbon Cycle Sciences NNX08AJ37G and NNX11AH20G and NSF ARC IPY #0732735.

References

Arp, C. D., Jones, B. M., Urban, F. E., and Grosse, G.: Hydrogeomorphic processes of thermokarst lakes with grounded-ice and floating-ice regimes on the Arctic coastal plain, Alaska, Hydrol. Process., 25, 2422–2438, doi:10.1002/hyp.8019, 2011.

Arp, C. D., Jones, B. M., Lu, Z., and Whitman, M. S.: Shifting balance of thermokarst lake ice regimes across the Arctic Coastal Plain of northern Alaska, Geophys. Res. Lett., 39, L16503, doi:10.1029/2012gl052518, 2012.

Boereboom, T., Depoorter, M., Coppens, S., and Tison, J.-L.: Gas properties of winter lake ice in Northern Sweden: implication for carbon gas release, Biogeosciences, 9, 827–838, doi:10.5194/bg-9-827-2012, 2012.

Brown, L. C. and Duguay, C. R.: The response and role of ice cover in lake-climate interactions, Prog. Phys. Geogr., 34, 671–704, doi:10.1177/0309133310375653, 2010.

Cloude, S. R. and Pottier, E.: A review of target decomposition theorems in radar polarimetry, IEEE T. Geosci. Remote, 34, 498–518, 1996.

Duguay, C. R., Pultz, T. J., Lafleur, P. M., and Drai, D.: RADARSAT backscatter characteristics of ice growing on shallow sub-Arctic lakes, Churchill, Manitoba, Canada, Hydrol. Process., 16, 1631–1644, doi:10.1002/hyp.1026, 2002.

Duguay, C. R., Flato, G. M., Jeffries, M. O., Menard, P., Morris, K., and Rouse, W. R.: Ice-cover variability on shallow lakes at high latitudes: model simulations and observations, Hydrol. Process., 17, 3465–3483, doi:10.1002/hyp.1394, 2003.

Elachi, C., Bryan, M. L., and Weeks, W. F.: Imaging radar observations of frozen arctic lakes, Remote Sens. Environ., 5, 169–175, doi:10.1016/0034-4257(76)90047-x, 1976.

TCD
7, 2061–2088, 2013

Engram, M., Anthony, K. W., Meyer, F. J., and Grosse, G.: Synthetic aperture radar (SAR) backscatter response from methane ebullition bubbles trapped by thermokarst lake ice, Can. J. Remote Sens., 38, 667–682, doi:10.5589/m12-054, 2012.

French, N., Savage, S., Shuchman, R., Edson, R., Payne, J., and Josberger, E.: Remote sensing of frozen lakes on the North Slope of Alaska, Geoscience and Remote Sensing Symposium, 2004, IGARSS '04, Proceedings, IEEE International, 3005, 3008–3011, 2004.

Gao, G.: Statistical modeling of SAR images: a survey, Sensors, 10, 775–795, doi:10.3390/s100100775, 2010.

Gow, A. J. and Langston, D.: Growth history of lake ice in relation to its stratigraphic, crystalline and mechanical structure, US Army, Corps of Engineers, Cold Regions Research and Engineering Laboratory, Hanover, New Hampshire, 24 pp., 1977.

Grosse, G., Jones, B., and Arp, C.: 8.21 Thermokarst lakes, drainage, and drained basins, in: Treatise on Geomorphology, edited by: John, F. S., Academic Press, San Diego, 325–353, 2013.

Hall, D. K., Fagre, D. B., Klasner, F., Linebaugh, G., and Liston, G. E.: Analysis of ERS-1 synthetic-aperture-radar data of frozen lakes in northern Montana and implications for climate studies, J. Geophys. Res.-Oceans, 99, 22473–22482, 1994.

Hirose, T., Kapfer, M., Bennett, J., Cott, P., Manson, G., and Solomon, S.: Bottomfast ice mapping and the measurement of ice thickness on tundra lakes using C-band synthetic aperture radar remote sensing, J. Am. Water Resour. As., 44, 285–292, doi:10.1111/j.1752-1688.2007.00161.x, 2008.

Hopkins, D. M.: The Espenberg Maars: a record of explosive volcanic activity in the Devil Mountain-Cape Espenberg area, Seward Peninsula, Alaska, in: The Bering Sea Land Bridge National Preserve: an Archeological Survey, edited by: Schaaf, J. M., National Park Service, Alaska Regional Office, 262–321, 1988.

Jeffries, M. O., Morris, K., Weeks, W. F., and Wakabayashi, H.: Structural and stratigraphic features and ERS-1 synthetic-aperture radar backscatter characteristics of ice growing on shallow lakes in NW Alaska, winter 1991–1992, J. Geophys. Res.-Oceans, 99, 22459–22471, 1994.

Jeffries, M. O., Morris, K., and Liston, G. E.: A method to determine lake depth and water availability on the north slope of Alaska with spaceborne imaging radar and numerical ice growth modelling, Arctic, 49, 367–374, 1996.

TCD
7, 2061–2088, 2013

Jeffries, M. O., Morris, K., and Duguay, C. R.: Lake ice growth and conductive heat flow in central Alaska, Arctic Science Conference Abstracts, 53, 120, 2002.
Jones, B. M.: Spatiotemporal Analysis of Thaw Lakes and Basins, Barrow Peninsula, Arctic Coastal Plain of Northern Alaska, MA, Department of Geography, University of Cincinnati, Cincinnati, 105 pp., 2006.
Jorgenson, M. T. and Shur, Y.: Evolution of lakes and basins in northern Alaska and discussion of the thaw lake cycle, J. Geophys. Res.-Earth, 112, F02S17, doi:10.1029/2006jf000531, 2007.
Jorgenson, T., Yoshikawa, K., Kanevskiy, M., Shur, Y., Romanovsky, V. E., Marchenko, S., Grosse, G., Brown, J., and Jones, B. M.: Permafrost Characteristics of Alaska, Permfrost map of Alaska, Ninth International Conference on Permafrost at University of Alaska Fairbanks, 2008.
Leconte, R., Daly, S., Gauthier, Y., Yankielun, N., Bérubé, F., and Bernier, M.: A controlled experiment to retrieve freshwater ice characteristics from an FM-CW radar system, Cold Reg. Sci. Technol., 55, 212–220, doi:10.1016/j.coldregions.2008.04.003, 2009.
Lee, J.-S. and Pottier, E.: Polarimetric Radar Imaging: From Basics to Applications, CRC Press Taylor & Francis Group, Boca Raton, FL, 2009.
Mellor, J.: Bathymetry of Alaskan Arctic Lakes: a key to resource inventory with remote sensing methods, PhD thesis, Institute of Marine Science, University of Alaska, 1982.
Morris, K., Jeffries, M. O., and Weeks, W. R.: Ice processes and growth history on Arctic and sub-arctic lakes using ERS-1 SAR data, Polar Rec., 31, 115–128, 1995.
Sellmann, P. V., Weeks, W. F., and Campbell, W. J.: Use of Side-Looking Airborne Radar to Determine Lake Depth on the Alaskan North Slope, Special Report No. 230, Cold Regions Research and Engineering Laboratory, Hanover, New Hampshire, 1–10, 1975.
Skolunov, A. V.: Frequency-temperature curve of the complex dielectric constant and refractive index of water, Fibre Chem., 29, 367–373, 1997.
Ulaby, F. T., Moore, R. K., and Fung, A. K.: Radar Remote Sensing and Surface Scattering and Emission Theory, Microwave Remote Sensing: Active and Passive, edited by: Ulaby, F. T., Artech House, Inc., Norwood, Mass., 608 pp., 1982, 1986.
van Zyl, J. J. and Kim, Y.: Synthetic Aperture Radar Polarimetry, 1st edn., JPL Space Science and Technology Series, edited by: Yuen, J. H., John Wiley & Sons Inc., Hoboken, New Jersey, 288 pp., 2010.

TCD
7, 2061–2088, 2013

Walsh, S. E., Vavrus, S. J., Foley, J. A., Fisher, V. A., Wynne, R. H., and Lenters, J. D.: Global patterns of lake ice phenology and climate: model simulations and observations, J. Geophys. Res.-Atmos., 103, 28825–28837, doi:10.1029/98jd02275, 1998.

Walter Anthony, K. M. and Anthony, P.: Constraining spatial variability of methane ebullition in thermokarst lakes using point-process models, J. Geophys. Res.-Biogeo., accepted, 2013.

Walter Anthony, K. M., Anthony, P., Grosse, G., and Chanton, J.: Geologic methane seeps along boundaries of Arctic permafrost thaw and melting glaciers, Nat. Geosci., 5, 419–426, doi:10.1038/ngeo1480, 2012.

Weeks, W. F., Sellmann, P., and Campbell, W. J.: Interesting features of radar imagery of ice covered north slope lakes, J. Glaciol., 18, 129–136, 1977.

Weeks, W. F., Fountain, A. G., Bryan, M. L., and Elachi, C.: Differences in radar return from ice-covered north slope lakes, J. Geophys. Res., 83, 4069–4073, 1978.

Weeks, W. F., Gow, A. J., and Schertler, R. J.: Ground-truth observations of ice-covered North Slope lakes imaged by radar, Report No. 81–19, Cold Regions Research and Engineering Laboratory, Hanover, New Hampshire, 1–17, 1981.

West, J. J. and Plug, L. J.: Time-dependent morphology of thaw lakes and taliks in deep and shallow ground ice, J. Geophys. Res.-Earth, 113, F01009, doi:10.1029/2006jf000696, 2008.

White, D. M., Prokein, P., Chambers, M., Lilly, M. R., and Toniolo, H.: Use of synthetic aperture radar for selecting Alaskan lakes for winter water use, J. Am. Water Resour. As., 44, 276–284, doi:10.1111/j.1752-1688.2007.00160.x, 2008.

TCD
7, 2061–2088, 2013

Table 1. SAR data were selected based on data availability over two study areas for late March/April from 1993 through 2011.

Region	L-band SAR (~ 24 cm wavelength, ~ 1.27 GHz)				C-band SAR (~ 5.7 cm wavelength, ~ 5.3 GHz)			
	SAR Platform/Mode	Date	Polarization	Theta	SAR Platform	Date	Polarization	Theta
ACP	JERS-1	1 Apr 1993	HH	40°	ERS-1	31 Mar 1993	VV	23°
ACP	JERS-1	5 Apr 1996	HH	39°	ERS-2	2 Apr 1996	VV	23°
ACP	JERS-1	24 Apr 1998	HH	40°	ERS-2	23 Apr 1998	VV	23°
ACP	PALSAR/Fine Beam Single-Pol	23 Mar 2008	HH	39°	ERS-2	25 Mar 2008	VV	23°
ACP	PALSAR/Fine Beam Single-Pol	9 Apr 2008	HH	39°	ERS-2	8 Apr 2008	VV	23°
ACP	PALSAR/Fine Beam Quad-Pol	23 Mar 2009	HH, HV, VH, VV	24°	ERS-2	24 Mar 2009	VV	23°
ACP	PALSAR/Fine Beam Single-Pol	29 Mar 2010	HH	39°	ERS-2	30 Mar 2010	VV	23°
ACP	PALSAR/Fine Beam Single-Pol	15 Apr 2010	HH	39°	ERS-2	15 Apr 2010	VV	23°
ACP	PALSAR/Fine Beam Quad-Pol	29 Mar 2011	HH, HV, VH, VV	24°	ERS-2	29 Mar 2011	VV	23°
NSP	JERS-1	11 Apr 1993	HH	40°	ERS-1	30 Apr 1993	VV	23°
NSP	JERS-1	20 Mar 1998	HH	40°	ERS-2	13 Apr 1998	VV	23°
NSP	PALSAR/Fine Beam Quad-Pol	24 Mar 2007	HH, HV, VH, VV	24°	ERS-2	28 Mar 2007	VV	23°
NSP	PALSAR/Fine Beam Single-Pol	26 Mar 2008	HH	24°	ERS-2	31 Mar 2008	VV	23°
NSP	PALSAR/Fine Beam Quad-Pol	29 Mar 2009	HH, HV, VH, VV	24°	ERS-2	29 Mar 2009	VV	23°
NSP	PALSAR/Fine Beam Single-Pol	30 Mar 2010	HH	39°	ERS-2	5 Apr 2010	VV	23°
NSP	PALSAR/Fine Beam Single-Pol	1 Apr 2010	HH	24°				

TCD
7, 2061–2088, 2013

Table 2. Summary of mean SAR backscatter intensity (dB) from floating and grounded lake ice for C- and L-bands from both study regions.

	C-band VV $\theta \approx 23^{\circ}$		L-band HH $\theta \approx 24^{\circ}$ or $\theta \approx 39^{\circ}$		L-band $T11$ (Roughness) $\theta \approx 24^{\circ}$		L-band $T22$ (Double Bounce) $\theta \approx 24^{\circ}$		L-band $T33$ (Volumetric) $\theta \approx 24^{\circ}$	
	Mean	n[a]	Mean	n[a]	Mean	n[a]	Mean	n[a]	Mean	n[a]
Floating Ice backscatter intensity										
Arctic Coastal Plain (ACP)	−6[b]	25	−16	19	−12	5	−17	5	−21	5
Northern Seward Peninsula (NSP)	−6[b]	24	−13	19	−9	8	−20	8	−24	8
Grounded Ice backscatter Intensity										
Arctic Coastal Plain (ACP)	−15	27	−19[b]	14	−16[b]	5	−20	5	−25[b]	5
Northern Seward Peninsula (NSP)	−14	19	−19[b]	21	−16[b]	7	−23	7	−27[b]	7

[a] Sum of sampled lakes counted from each SAR scene.
[b] Denotes that a t test failed to reveal a statistically significant difference between the mean backscatter from the ACP and the NSP.

TCD
7, 2061–2088, 2013

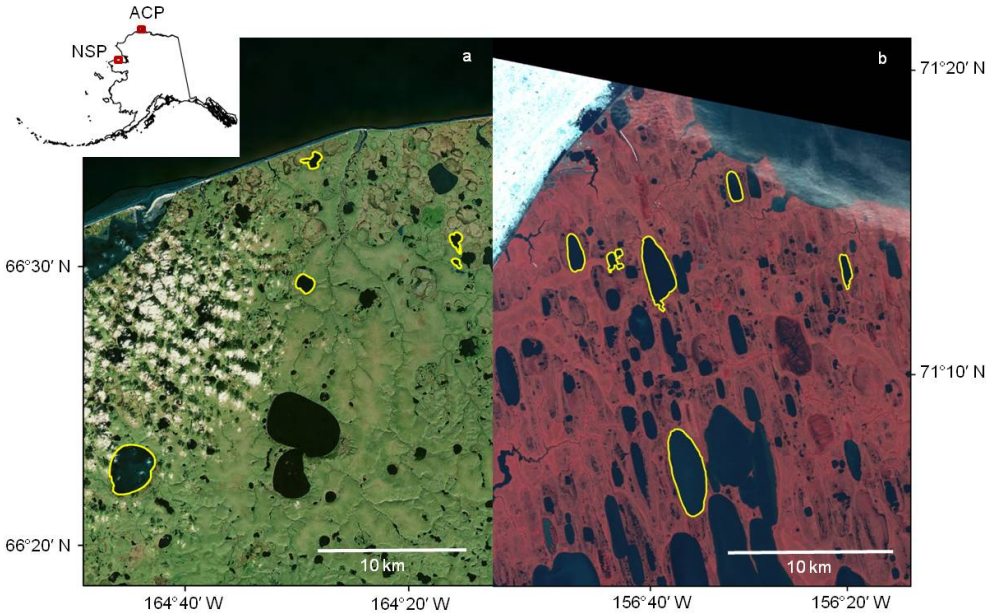

Fig. 1. Study lakes are highlighted in yellow on **(a)** northern Seward Peninsula (NSP) and **(b)** Arctic Coastal Plain (ACP) south of Barrow. In **(a)** the large lake in the lower left is Whitefish Maar and the double-lobed lake in the center bottom is Devil Mountain Maar, both of volcanic origin; all other study lakes in both regions are of thermokarst origin. **(a)** Is a Landsat mosaic from the Geographic Information Network of Alaska and **(b)** is a scene from 10 July 2008 AVNIR-2 (Advanced Visible and Near Infrared Radiometer type 2).

TCD
7, 2061–2088, 2013

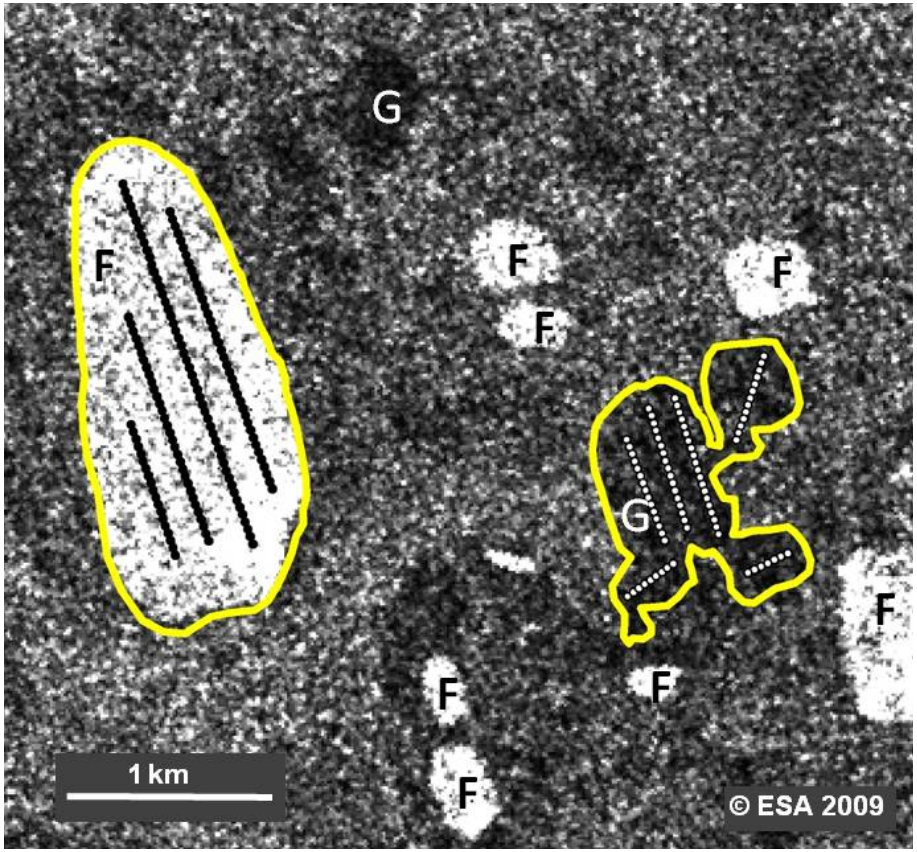

Fig. 2. C-band VV SAR image of thermokarst lakes on the Arctic Coastal Plain (ACP), Alaska. High backscatter from floating lake ice is indicated by "F" while low backscatter from grounded lake ice is indicated by "G". Two study lakes are outlined in yellow and pixel sampling locations are rows of uniformly spaced points, shown in contrasting color.

TCD
7, 2061–2088, 2013

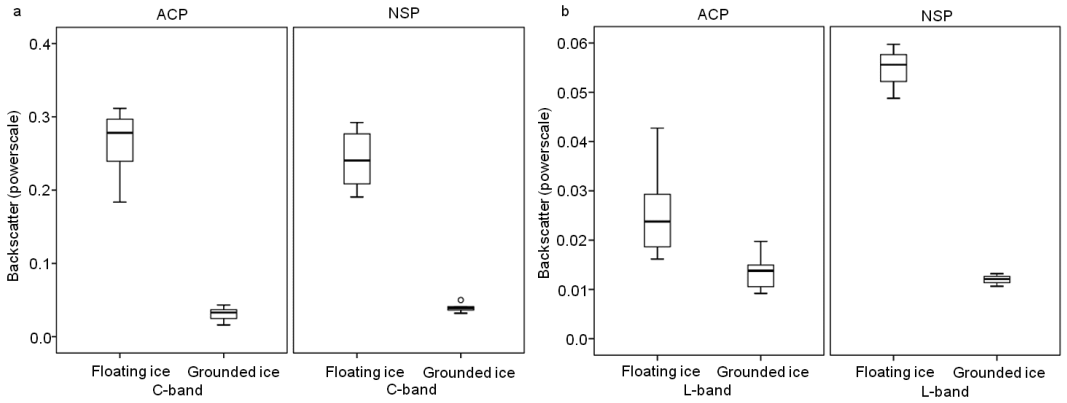

Fig. 3. Boxplots of the mean backscatter value of all floating and grounded ice for each SAR scene from **(a)** C-band and **(b)** L-band. No statistical far-outliers and only one near outlier (**a**: NSP, ERS-1, 30 April 1993) indicate that SAR backscatter values from floating and grounded ice in late March/April are similar from year to year. Note different scales on Y-axis for **(a)** and **(b)**.

TCD
7, 2061–2088, 2013

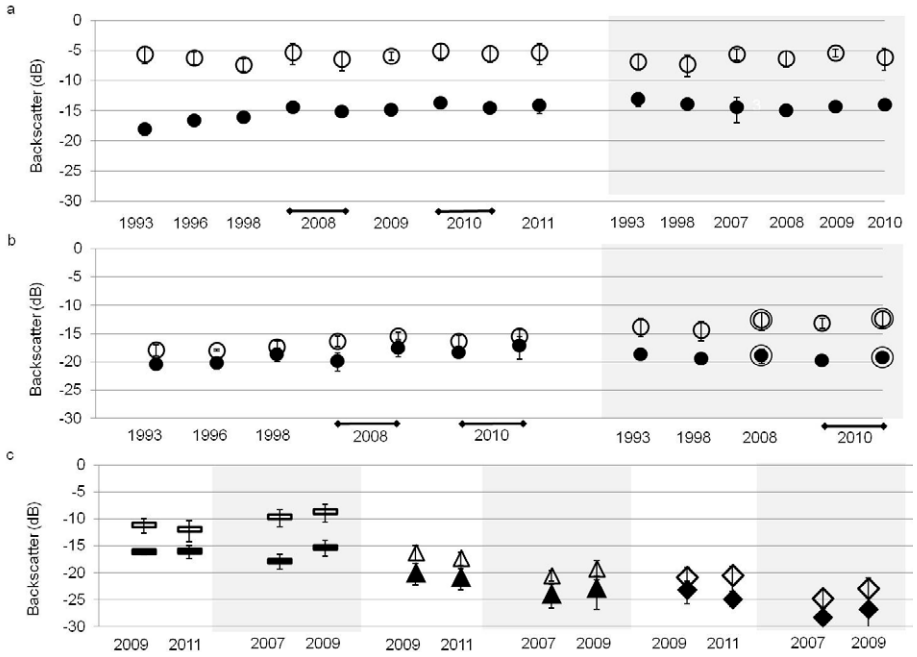

Fig. 4. Mean SAR intensity backscatter values in decibels from floating lake ice (open symbols) and grounded lake ice (closed symbols) from **(a)** C-band VV from ERS-1 and ERS-2, **(b)** L-band HH from JERS-1 and PALSAR, **(c)** L-band quad-pol from PALSAR coherency matrix elements $T11$ (rectangles), $T22$ (triangles) and $T33$ (diamonds) that indicate double-bounce, volumetric scattering, and roughness, respectively. Incidence angles are **(a)** 23°, **(b)** 39–40°, except 24° as noted by concentric circles, **(c)** 24°. Shaded areas highlight lake ice from the northern Seward Peninsula (NSP) and white areas highlight lake ice from the Alaska Arctic Coastal Plain (ACP). Mean backscatter values are from spring lake ice (late March/April) from study lakes outlined in Fig. 1. Error bars represent standard deviation.

TCD
7, 2061–2088, 2013

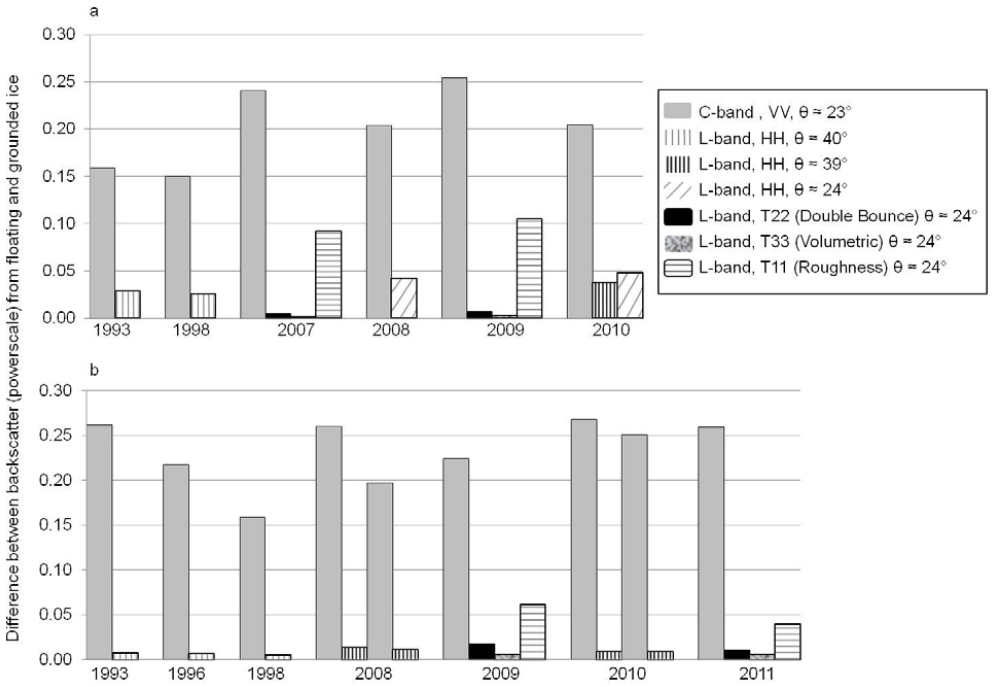

Fig. 5. Difference in SAR intensity between floating and grounded ice for **(a)** northern Seward Peninsula (NSP) and **(b)** Arctic Coastal Plain (ACP). C-band clearly shows a larger difference between floating and grounded ice for both regions. The *T*11 component from polarimeteric decomposition of quad-pol L-band data indicates that roughness is the dominant scattering mechanism for floating ice for L-band, and is greater in NSP than ACP.

TCD
7, 2061–2088, 2013

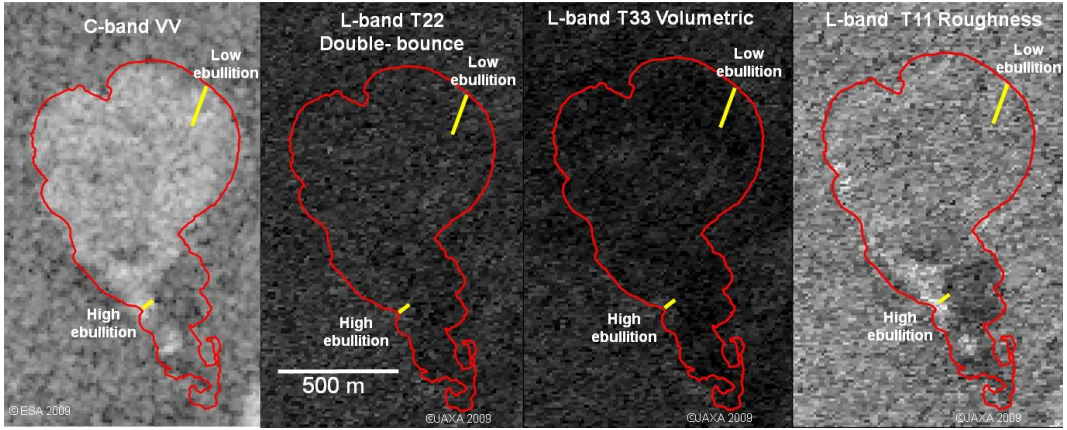

Fig. 6. A frozen thermokarst lake on the Seward Peninsula with floating ice on northern portion of lake and grounded ice at the southern portion shown in C-band VV and L-band $T11$, $T22$ and $T33$ images acquired on 29 March 2009. C-band VV shows the strongest contrast between floating and grounded lake ice. The $T11$ roughness component of quad-pol L-band shows some contrast between floating and grounded ice, but it also shows high absolute backscatter, seen as bright areas from high-methane ebullition areas, as determined by field measurements (yellow lines) in October 2008 (Engram et al., 2012).

TCD
7, 2061–2088, 2013